



TECHNICAL ARTICLE

Effect of Pre-corrosion Damage on Dry Sliding Wear Behavior of Differently Heat-Treated Martensitic Stainless Steel

Neelima Khare, Sunil Kumar Bonagani, P.K. Limaye, Naveen Kumar, and Vivekanand Kain

Submitted: 18 September 2022 / Revised: 13 February 2023 / Accepted: 18 February 2023 / Published online: 8 March 2023

This study explored the effect of pre-corrosion damage on the tribology behavior of the austenitized and the different tempered conditions of 13 wt.% Cr martensitic stainless steel under dry sliding conditions using a “ball on plate” configuration. Corrosion immersion experiments were performed in 5 wt.% HNO₃ solution at room temperature for 30 min. The austenitized and the tempered at 300 °C (T300) specimens displayed the attack along the prior austenitic grain boundaries, whereas the specimens tempered at 550 (T550) and 700 °C (T700) showed intergranular plus interlath corrosion and uniform corrosion, respectively. Subjecting this corrosion-damaged specimens to dry sliding revealed non-monotonic friction and wear behavior with tempering temperature. The microstructure and the type of corrosion attack together determined the overall wear performance of the tempered conditions. The specific wear rate (k) decreased in the order $k_{T700} > k_{T550} > k_{T300} \sim k_{\text{austenitized}}$. The k value of the austenitized and the T300 specimens ($\sim 32 - 35 \times 10^{-6} \text{ mm}^3/\text{Nm}$) is observed to be 12 and 15 times lower than the k value of T550 ($\sim 408 \times 10^{-6} \text{ mm}^3/\text{Nm}$) and T700 ($\sim 495 \times 10^{-6} \text{ mm}^3/\text{Nm}$) specimens, respectively. The reason for the lower k value is due to the continuous, thick ($\sim 4 \mu\text{m}$ thickness) Cr-rich tribo-film that formed on the wear track and acted as solid lubricant. The T550 and T700 specimens had a discontinuous Fe-rich tribo-film on the wear tracks; therefore, rubbing in the presence of harder and loose Fe-rich oxides particles led to severe adhesion plus galling in T550 and smearing plus plastic deformation in T700 specimens. It was also found that the wear rate and surface damage are reduced for pre-corroded austenitized and T300 specimens compared to the respective unattacked pristine specimens; however, the opposite effect was observed in T550 and T700 specimens.

Keywords coefficient of friction, martensitic stainless steel, pre-corrosion damage, tribo-films, wear

1. Introduction

Martensitic stainless steels (MSSs) are widely used in different industries including nuclear because of their better mechanical properties, combined with good corrosion and wear resistance (Ref 1-3). The corrosion resistance of SSs originates from a thin (of a few nm thicknesses) passive film composed of Cr₂O₃ or Cr-containing spinel type oxide (FeCr₂O₄/NiCr₂O₄)

with a self-healing property (Ref 4, 5). This passive film prevents the interaction of the base material with the environment and thus, protects it from the environment. The breakage of the passive film depends on the chemical composition and microstructure of the material and also on the environment. For examples, SSs undergo pitting corrosion in chloride solutions due to collapse of the passive film locally and the intergranular corrosion (IGC) due to the breakage of the weaker passive film formed at the Cr-depleted regions near the grain boundaries (Ref 6, 7).

The protective film may rupture and then, allow the material to be damaged tribologically either during dry sliding (in air) or under mild acidic lubrication (Ref 8, 9). It is well known that the heat generated during the frictional contacts promotes the formation of tribo-films (of different nature and thickness). These tribo-films are reported to be capable of preventing the direct contact of the SS surface with its counterpart and play a vital role in modifying the wear & friction characteristics (Ref 10-13). Therefore, increasing efforts have been made to understand the effects of evolution of surface oxidation and surface layers on the friction and wear properties of steels and SSs in different microstructural conditions (Ref 11-14). The tribo-films of SSs, generated under dry sliding conditions, were composed of oxide particles such as Fe₂O₃, FeCr₂O₄ (FeO + Cr₂O₃), and Fe₂SiO₄. (Ref 13, 14). These oxide particles have the tendency to undergo mixing and compaction under the contact stresses between the mating surfaces and act as either a solid lubricant or abrasive agent (Ref 15, 16). Therefore,

Neelima Khare, Reactor Technology Division, Bhabha Atomic Research Centre, Trombay, Mumbai 400085 India; and Homi Bhabha National Institute, Anushaktinagar, Mumbai 400094, India; **Sunil Kumar Bonagani**, Materials Processing and Corrosion Engineering Division, Bhabha Atomic Research Centre, Trombay, Mumbai 400085, India; **P.K. Limaye**, Reactor Technology Division, Bhabha Atomic Research Centre, Trombay, Mumbai 400085 India; **Naveen Kumar**, Materials Science Division, Bhabha Atomic Research Centre, Trombay, Mumbai 400085, India; and **Vivekanand Kain**, Materials Processing and Corrosion Engineering Division, Bhabha Atomic Research Centre, Trombay, Mumbai 400085, India; and Homi Bhabha National Institute, Anushaktinagar, Mumbai 400094, India. Contact e-mails: neelimak@barc.gov.in and bsunil@barc.gov.in.

surface oxide layer formed on the steel surface can change the tribological characteristics of the lubrication (Ref 17). Solid lubricants help to reduce friction and wear of steels (Ref 13, 14), whereas abrasive agents act as stress raisers and can result in higher wear and fluctuating friction (Ref 12). If the oxide debris formed is free and harder & brittle in nature, then abrading behavior was noticed, whereas the adhered oxide scale formed uniformly over the surface, decreased the metal-on-metal contact during the dry coupling of metallic parts (Ref 13, 14). Because of this, depending on the kind of the lubricating agent generated during the wear process, both detrimental and beneficial effects of the tribo-films were observed. Chen et al. (Ref 14) reported an improvement in wear resistance of martensite steel in dry sliding conditions due to the formation of films composed of Fe_2O_3 , Cr_2O_3 and FeCr_2O_4 on the worn surfaces.

It was also reported that the lubrication offered by the oxide layer is linked to the evolution of the subsurface microstructural developments during the dynamic sliding friction process (Ref 16). The stress fields and heat generated within the frictional contacts can induce the deformation in subsurface and alter the initial microstructure. The effect of sliding wear-induced subsurface modifications and oxidation on tribological performance was studied in a few materials (Ref 16-22). In a review by Jacobson et al. (Ref 17) on different tribo-systems concluded that the surface and subsurface modifications of plate material are inevitable during dry or boundary lubricated tribological contacts. The modifications may include topographical changes such as smoothing or roughing, formation of micro-cracks, oxides, solid films, deformation hardening, and the transfer of material from the counter surface. Mashuko et al. (Ref 18) reported superior tribological performance for SS 440C when oxide layer is present.

Currently available literature on tribocorrosion of different MSSs highlights their behavior in chloride containing environments (Ref 23). The nitric acid-based solutions have been used for cleaning, descaling and passivation treatments of stainless steels. The acid concentrations used in such operations are shown to be sufficient enough to cause IGC in quenched & tempered MSSs even at room temperature (Ref 1, 7). However, no tribological studies are reported in such environments. Therefore, understating the wear behavior of MSSs in such circumstances (i.e., IGC attacked/undergoing IGC during in-service) is a topic of paramount relevance and helpful for selection of materials.

Recently, it has been shown that the microstructural changes induced by the tribological loadings affected the localized corrosion behavior of MSSs and is reported to be dependent on the number of cycles (Ref 24). In a recent work, it was also observed that the MSS tempered at 550 °C condition which has the least wear resistance to dry sliding had shown the lowest specific wear rate in nitric acid (HNO_3) sliding conditions (Ref 9). The surface films developed under HNO_3 sliding conditions are shown to be Fe-rich oxides and acted as solid lubricant and shielded the substrate contact with the environment. However, HNO_3 trapped locations inside the wear track caused the enhanced localized corrosion attack (Ref 8, 9). The wear can accelerate the corrosion mainly by (a) breakage of passive film, (b) sub-surface microstructural changes/plastic deformation thereby increase in the dislocation density and (c) generation of surface irregularities (Ref 24-26).

Practically, engineering materials might undergo corrosion before deployment into tribological applications either due to

manufacturing processes (e.g., pickling in HNO_3) or due to material-environment interactions (e.g., oxidation, rusting). Incidences of occurrence of IGC in valve and stem materials made of 13 wt.% Cr MSSs, due to fabrication process, have been reported (Ref 27, 28). Wear studies of such conditions are of practical importance, and data generated are very useful for designers and engineers. To the authors' knowledge, no studies have yet been reported on the tribological behavior of tempered 13 wt.% Cr MSS (in corrosion attacked conditions) under dry sliding conditions. Investigating such effects on the wear behavior will contribute to the basic understanding of the complex phenomenon of tribocorrosion. Indeed, we are currently performing the tribocorrosion behavior of these conditions and, the results obtained so far are very insightful in understanding and explaining the complex tribocorrosion behavior of MSSs.

Some machine components slide under corrosive lubrication environments and display synergistic phenomena of tribocorrosion due to in situ occurrences of wear and corrosion. Whereas in dry sliding, the protective oxide films may form directly on stainless steels to provide resistance to wear (in non-corroded conditions). The composition and continuity of the developed oxide layers on stainless steels in dry sliding contacts play a significant role on their tribological behavior. These layers can either act as solid lubricant thereby improve friction and wear performance or act as a stress raiser and degrade the wear performance (Ref 12, 13). The dry sliding of corroded conditions is expected to exhibit different wear performance compared to that of non-corroded conditions under identical conditions. Since, the nature and continuity of oxide layers developed on the corroded surfaces may totally different to that of non-corroded surfaces and wide differences in their wear and friction behavior are anticipated. The present work mainly highlights the role of such layers (presented on corroded materials) on friction and wear behavior. Also, it brings out the wear performance in pre-corrosion-damaged conditions in dry sliding conditions.

Therefore, in the present study, a systematic investigation has been carried out to understand the tribological behavior of the austenitized and the tempered (at 300, 550 and 700 °C) 13 wt.% Cr MSS in corrosion attacked conditions. Room temperature immersion tests in 5 wt.% HNO_3 solution were conducted to establish the corrosion behavior of the austenitized and the different tempered conditions. These attacked specimens were subjected to tribology tests using ball-on-plate configuration. The developed wear track regions were characterized in-detail and compared to that of respective unattacked specimens to find out any synergistic/mutual dependence of mechanical and corrosion effects.

The findings of the study offer a better understanding on the application of tempered MSSs in corrosion attacked conditions, which is helpful in the selection of materials involving both wear and corrosion. It is to be noted that the corrosion behavior of 13 wt.% Cr MSS in 5 wt.% HNO_3 solution was evaluated for shorter duration, i.e., for 30 min and is reported for the first time. In one of the author's previous studies, the corrosion behavior was reported after immersion for 24 h (Ref 8) and also oil-quenching was used in the austenitization treatment whereas in the present study air cooling was used (Ref 8). For the first time, the wear behavior of pre-corrosion-damaged conditions of the austenitized, the T300 and T700 conditions, is reported and compared with behavior of T550 condition reported in (Ref 9)

and also compared with that of its unattacked counterpart conditions.

2. Experimental Details

2.1 Material, Heat Treatments and Characterization

The chemical composition of the as-received 13 wt.% Cr MSS used in the present investigation was analyzed using spark optical emission spectroscopy and is tabulated in Table 1. The specimens of size 20 mm (L) × 20 mm (W) × 5 mm (T) were cut from the as-received condition. These cut specimens were austenitized at 1020 °C for 30 min followed by air cooling, subsequently, tempered at 300, 550 and 700 °C for a period of 2.5 h. The detailed procedure and selection of temperatures and duration were provided in author's previous work (Ref 9). In the subsequent sections, the tempered specimens were designated as T300, T550, and T700. Before tests, each specimen was wet ground successively up to 1200 grit emery papers and then, mirror-polished using 1 μm diamond paste followed by cleaning in soap solution and running water. The hardness and surface roughness measurements were performed on each mirror-polished austenitized and tempered specimens as per the procedures presented in our previous works (Ref 9, 29).

2.2 Immersion Corrosion Tests

The mirror-polished specimens, prepared as per Sect. 2.1, were exposed to 5 wt.% HNO₃ solution at room temperature for a period of 30 min. It is to be noted that the corrosion behavior of these conditions for shorter duration (30 min in our case) is not available in the reported literature. The initial and final weights of the specimens were recorded with an accuracy of 1 μg, and corrosion rates were calculated in mpy using Eq 1.

$$\text{Corrosion Rate (CR)} = \frac{K * W}{A * T * \rho} \quad (\text{Eq 1})$$

where K is a constant (3.45×10^6), A is total surface area of exposed specimen in cm²; W is weight change in g; T is total time of immersion in h; ρ is density of the specimen in g/cc.

The immersion tests were repeated twice, and the average corrosion rate (along with standard deviation) was reported. Nature of the attack/damage was examined on exposed surfaces using field emission-scanning electron microscopy (FE-SEM) (Model and make: Auriga 4553, Carl Zeiss, Jena, Germany). The cross sections of the exposed specimens were prepared using ultra-precision cutting machine followed by hot mounting using a conductive resin. The mounted specimens were mirror-polished as per the metallographic procedure described in Sect. 2.1. The depth of the attack/damage was examined using FE-SEM.

Table 1 Chemical composition (all in wt.%) of 13 wt.% Cr MSS used in the present study

C	Cr	Mn	S	Ni	V	P	Cu	Fe
0.31	13.3	0.81	0.01	0.27	0.04	0.02	0.15	Bal.

2.3 Tribology Tests and Post-test Evaluations

The tribology experiments were performed as per ASTM G-99 using a standard Tribometer (Model& make: TR-20LE-M110, Ducom Instruments, Bangalore, India) with a “ball on plate” test configuration under dry sliding conditions. Alumina ball of 6 mm diameter was used as the counterface material due to its hard and inert nature. The mechanical properties of the plate in the austenitized and the different tempered conditions and alumina ball (supplier data) are provided in Table 2. These properties were used to calculate the Hertzian contact stress. Prior to the tribology test, the plate material was exposed to 5 wt.% HNO₃ solution for 30 min. The experimental parameters for dry sliding are as follows: test duration: 30 min, wear track diameter: 6 mm, applied load: 20 N, sliding speed: 0.005 m/s, sliding distance: 4.5 m, medium: dry at 25 °C, mode: unidirectional sliding. The reason for selecting the aforementioned test parameters is as follows: (a) wear track diameter was set to 6 mm to utilize the full surface area available on a test specimen, (b) applied load was 20 N as it produces the Hertzian contact stress (P) in the range of 2 GPa and is sufficient to maintain the localized damage in elasto-plastic zone (c) sliding speed maintained at very low level of ~ 0.005 m/s, since most of the components working in reactor environments move very slowly (due to high precision process requirements) and is rarely studied at such a low speeds, (d) test duration is kept at 30 min as this duration is long enough to cause corrosion attack and able to generate wear effects, (e) total sliding distance is about 4.5 m is calculated and depends on rpm, test duration and track diameter and (f) test mode was unidirectional sliding as in this mode of sliding, wear debris generally stays at the contact interface; hence, participation of debris in the friction, wear and corrosion process can be studied. Schematic of the test configuration, test parameters, procedure to calculate steady state coefficient of friction (COF) from online monitored data along with methods to evaluate wear depth and specific wear rates of plate and ball as per the standard procedures were described elsewhere in our previous works (Ref 9, 29).

Each test was repeated at least thrice on a fresh ball and plate specimen to ensure reproducibility. Schematic of test configuration, test parameters, procedure to calculate steady state COF from online monitored data along with methods to evaluate wear depth and specific wear rates of plate and ball as per the standard procedures were described elsewhere in our previous works (Ref 9, 29). The top surface of wear tracks on plate specimens was characterized using a FE-SEM equipped with energy-dispersive spectroscopy (EDS) (Model and make: X-Max, and Oxford, UK) and Raman spectroscopy (Model and

Table 2 Mechanical properties of the 13 wt.% Cr MSS plate and alumina ball (Supplier's data)

Property	Values	
	13Cr MSS	Alumina
Density (g/cc)	7.8	3.9
Elastic modulus (GPa)	200	375
Poisson's ratio	0.28	0.22
Yield strength, σ_y (MPa)	1200±26 (austenitized); 1133±91 (T300); 1022±58 (T550); 602±13 (T700)	

make: Invia-Reflex and Reinsaw, UK) to elucidate the wear mechanisms. Surface roughness (Ra) of each specimen (on and away from the wear track) was measured using a 3D optical profilometer (Model and make: Taylor Hobson CCI Optics, UK). Measurements were performed over an area of 0.25 mm² at three different locations on each specimen and average values (along with standard deviation) reported. Few selected plate specimens were cut from the middle of the wear track using slow speed precision cutting machine, and the cross sections of the cut plate specimens were hot mounted using a conductive resin. Mirror polishing of the mounted specimen was carried out to examine the subsurface degradation, if any, using an optical microscope and FE-SEM/EDS.

3. Results and Discussion

3.1 Changes in Localized Corrosion Behavior After the Austenitization and the Tempering Treatments

Figure 1 shows the corrosion rates (along with their standard deviation) for the austenitized and the different tempered conditions after exposure to 5 wt.% HNO₃ solution at room temperature for 30 min. The austenitized and the T300 conditions had almost same corrosion rates (755-968 mpy), whereas T550 and T700 conditions had corrosion rates of 5025 and 1780 mpy, respectively. The T550 condition showed the highest corrosion rate, whereas T300 condition showed the least corrosion rate. The examination of the top (longitudinal) and cross section of the exposed surfaces revealed different types of attack in the tempered conditions. The austenitized condition showed discrete attack along the PAG boundaries as shown in Fig. 2(a). The top surface examination revealed no evidence of grain drooping and also none of the martensitic laths preferentially got attacked during the exposure to 5 wt.% HNO₃ solution in the tested duration (Fig. 2(b)). However, the attacks along the carbide-matrix interface regions were observed as shown in Fig. 2(b) indicating the micro-chemical in-homogeneity at the interface regions. The discrete preferential attack along the PAGs is mainly due to the formation of Cr-rich carbides with concomitant Cr-depletion at carbide matrix interface regions at the PAGs during cooling from the

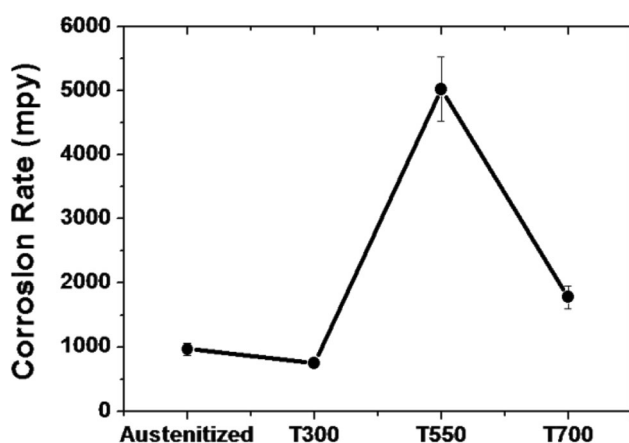


Fig. 1 Corrosion rate for the austenitized and the different tempered conditions after 30 min immersion in 5 wt.% HNO₃ solution

austenitization temperature (Ref 30-32). The cross-sectional examination of the exposed surface revealed attack depth of about 4.5 μm along the PAG boundary in the austenitized condition (Fig. 3a) which is less than the grain size, and so no grain drooping was observed. Similar morphological attack was seen in T300 specimen too. It was reported that the carbides formed after tempering at 300°C are Fe-rich, Fe₃C type carbides and formation of such carbides do not induce any Cr-depletion at the carbide-matrix interface regions. Therefore, the attack in T300 condition was observed only along the PAG boundaries in longitudinal (Fig. 2c and d) and cross-sectional examination of the exposed surfaces as shown in Fig. 3(b). In the present study, it was observed that the corrosion rate (968 mpy) of the austenitized condition that was cooled by air cooling is much higher than the corrosion rate reported for the austenitized condition that was cooled by oil quenching. This indicates that shorter durations are sufficient enough to cause sensitization in 13 wt.% Cr MSS during cooling to room temperature for the martensitic transformation. Figure 2(e) and (f) shows the unevenly attacked top surface of the T550 condition after exposing to 5 wt.% HNO₃ solution for 30 min. Similar type of surface features was reported in the literature after exposure to 5 wt.% HNO₃ solution for a period of 24 h and attributed to the preferential attack along the lath interfaces due to the presence of narrow Cr-depletion regions associated with nano-sized Cr-rich carbides (Ref 7).

In the present study, the cross-sectional examination of the exposed surface (Fig. 3c) of T550 specimen showed the preferential attack along the lath interfaces and the grain boundaries. The high rates of corrosion and the attack along the interfaces and uneven attack observed in T550 specimen confirm that it is in highly sensitized condition. The nano-sized Cr-rich carbides formed along the lath and PAG boundary interfaces are causing the preferential attack at the interfaces and also uneven surface (Ref 32). The corrosion rates observed for T700 are lower than T550 specimen but higher than the austenitized and T300 specimens (Fig. 1). This could be due to diffusion of Cr from the matrix to depleted regions associated with Cr-rich carbides and replenishing the Cr-depleted regions at 700 °C (Ref 7). The diffusion rate of Cr in ferritic/martensitic matrix is 10 times higher than in austenitic matrix, and shorter durations are sufficient for replenishing the Cr-depleted regions in martensitic SS (Ref 7). The examination of the longitudinal and cross-sectional surfaces revealed no preferential attack either along the PAG boundaries or along lath interfaces for T700 specimen as shown in Fig. 3(d). The higher corrosion rate observed for the T700 specimen is attributed to its lower Cr concentration in the matrix due to the formation of Cr-rich carbides at the lath interfaces (Ref 29), thus leading to weaker passivation in HNO₃ solution. Subjecting the 13 wt.% Cr MSS tempered at three different temperatures to HNO₃ solution, resulted in IGC along the PAG boundaries in T300 condition, IGC and interlath in T550 and heavy uniform corrosion in T700 condition as shown in Fig. 2. Naturally, the differences in corrosive attack could modify the surface appearance and the corresponding surface roughness.

3.2 Frictional Behavior

Figure 4(a) demonstrates the online monitored COF versus time curves for the austenitized and the tempered conditions (in corrosion attacked conditions), against counterface alumina ball. As shown in Fig. 4(a), starting COF (μ_s) before the onset

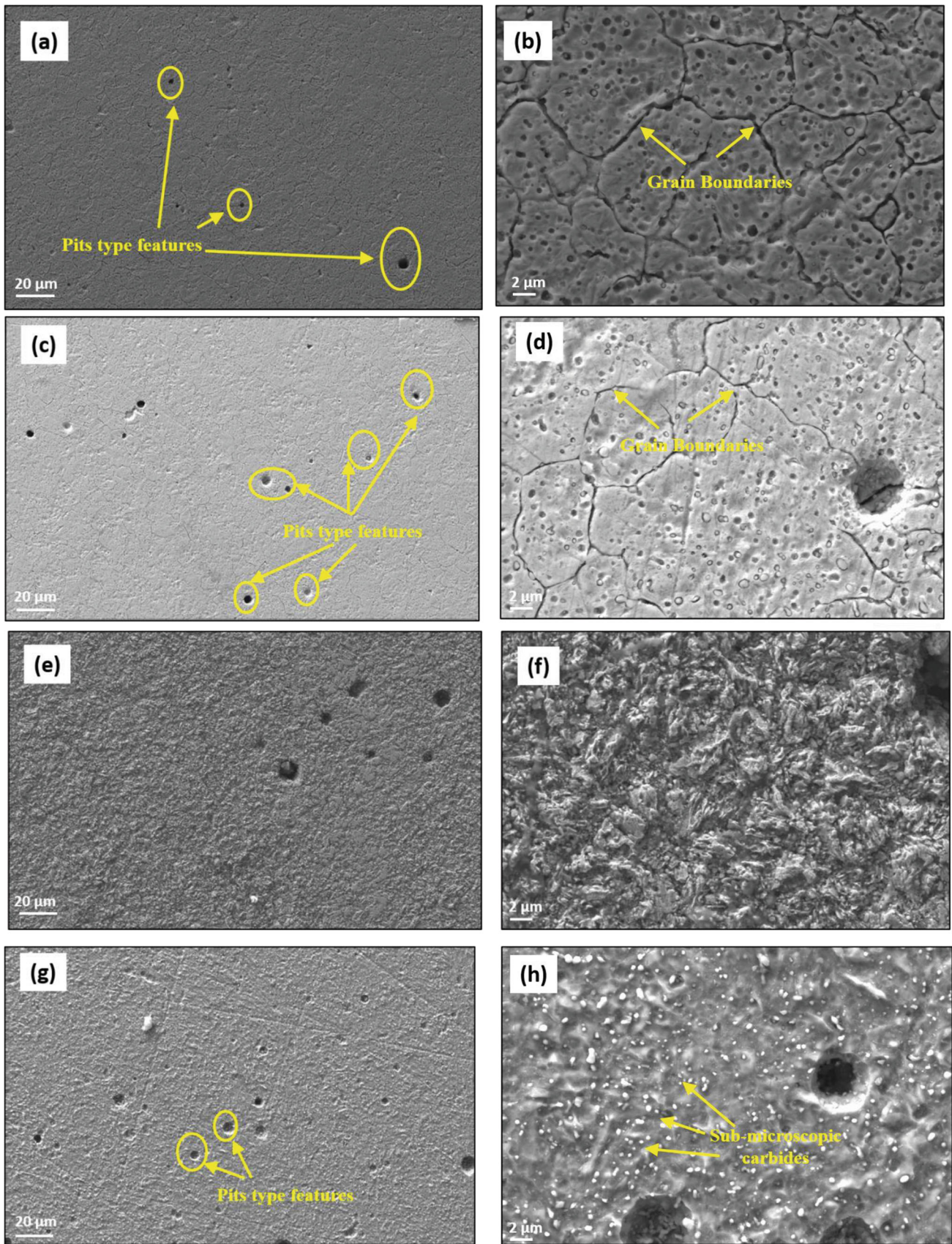


Fig. 2 FE-SEM images of 13 wt.% Cr MSS showing exposed surface after 30 min immersion in 5 wt.% HNO₃ solution, (a)-(b) Austenitized, (c)-(d) T300, (e)-(f) T550 and (g)-(h) T700

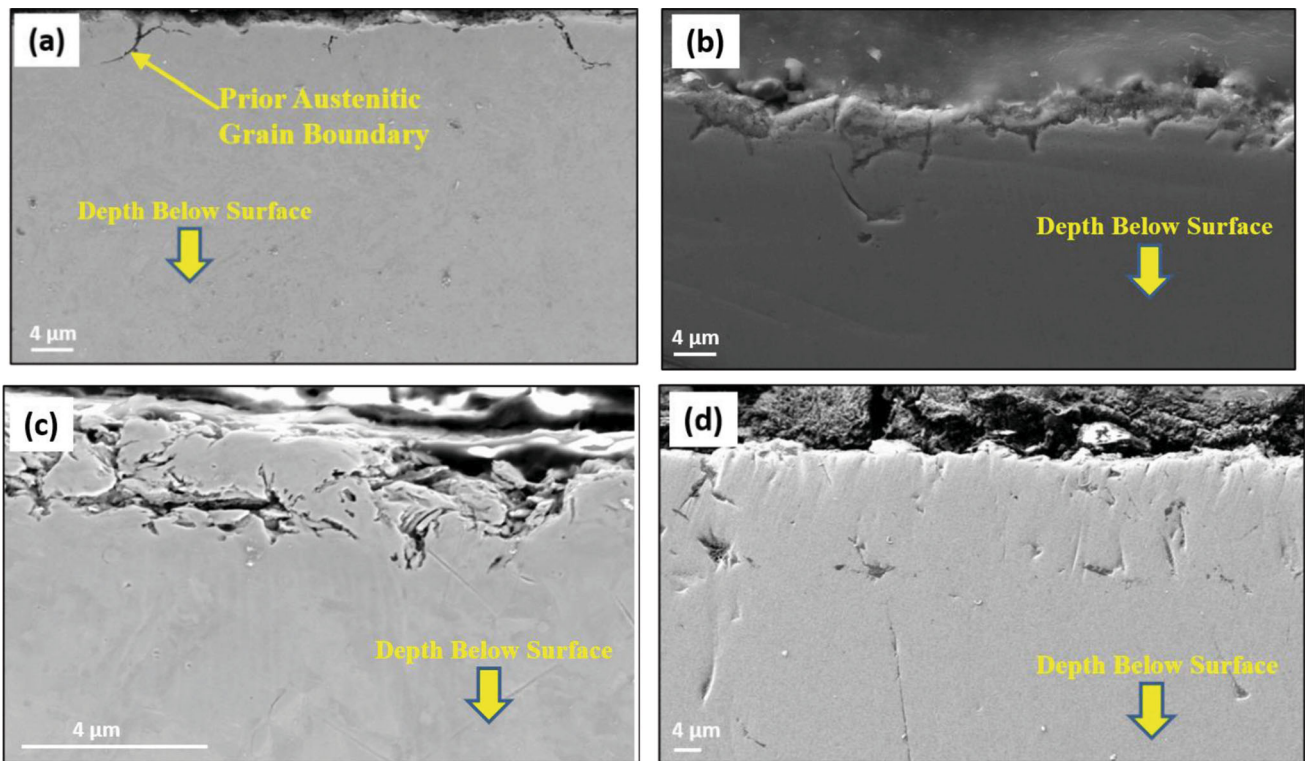


Fig. 3 FE-SEM images of 13 wt.% Cr MSS showing cross section of the exposed surface in 5 wt.% HNO₃ solution for 30 min, (a) Austenitized, (b) T300, (c) T550 and (d) T700

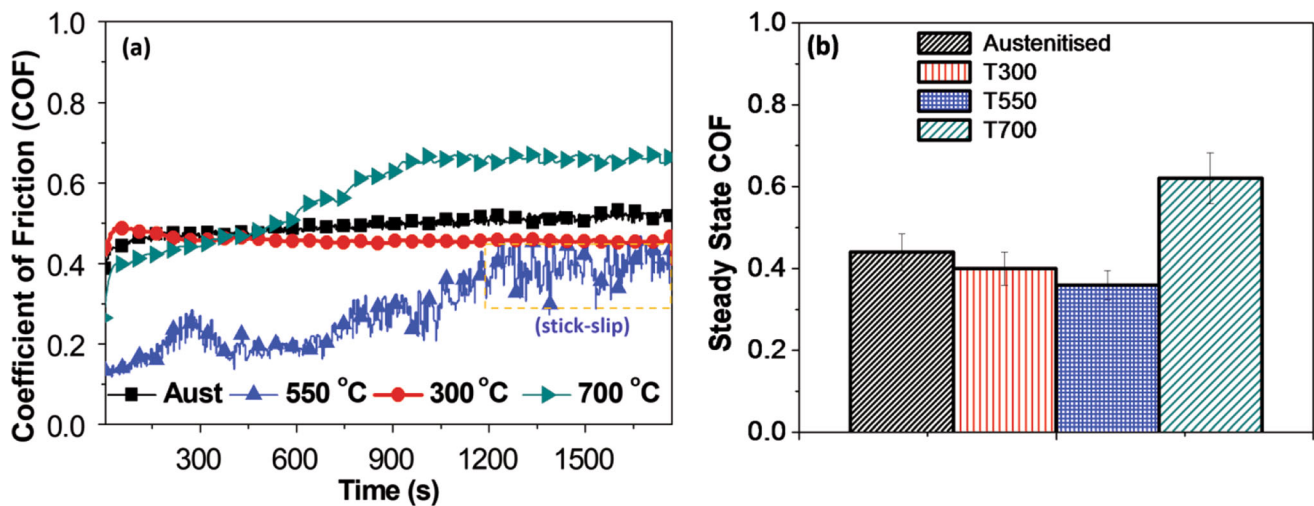


Fig. 4 (a) Online monitored coefficient of friction curves for 13 wt.% Cr MSS (in corrosion attacked condition) for the austenitized and the tempered conditions, dry sliding against alumina ball and (b) Average steady state coefficient friction value of the corresponding condition calculated from (a)

of sliding for the austenitized, T300 and T700 conditions is in very close range of ~ 0.38 - 0.41 , whereas the μ_s for T550 condition is about 0.18 . This is attributed to the differences in the initial surface roughness (R_a) of the studied conditions. The austenitized, T300 and T700 conditions after HNO₃ exposure had the R_a values of 120 nm, 110 nm and 160 nm, respectively, whereas the T550 condition had the R_a value of 440 nm. Therefore, the specimens with similar R_a values (along with same test conditions) generated almost the same μ_s . The increase in surface roughness leads to reduction in real contact

area between the sliding surfaces. This results into increase in local contact stresses at the asperity contacts and eventually reduces the ability of these asperity contacts to carry additional tangential load (before the onset of sliding); therefore, reduction in deformation component of friction yields lower COF (Ref 33-38).

In general, tribological contacts in dry sliding show fluctuations in COF during initial period of sliding and attain a stable COF after sliding for a sufficient duration. The austenitized and the T300 specimens attained steady state COF,

in about $t_s \sim 150$ s after the start of the experiment as shown in Fig. 4(a). Such a quick stable COF under dry sliding contacts is possible mainly due to the occurrence of either combined or the individual phenomenon of (a) negligible wear debris (third bodies) generation, (b) immediate formation/presence of stable tribo-film on the surface and (c) attainment of steady state condition in the generation and removal of wear debris (Ref 10, 13). The T700 specimen attained steady state COF, approximately after 950 s from start of the dry sliding and is the highest among all tested conditions. We believe, this is due to the longer time taken for the formation of a stable layer of debris on the track region (Ref 33). The T550 specimen showed fluctuations in COF, till end of the tribology experiment as shown in Fig. 4(a). The fluctuations/oscillations seen in the COF of T550 specimen with sliding distance are similar to that reported in well-known stick–slip phenomenon (Ref 34, 35). The stick–slip occurs due to periodic formation and breakage of asperity junctions during sliding and leads to micro-galling. Occurrence of stick–slip is usually reflected in (a) oscillations in COF with time (never attains steady state COF) and (b) generation of micro-galling features on worn-out surface (Ref 35–38). Indeed, the occurrence of micro-galling was confirmed through SEM examination of wear track of T550 specimen and is discussed in the Sect. 3.5. The calculated average steady state COF for the austenitized and the different tempered conditions is in the range of 0.36 to 0.62 and is presented in Fig. 4(b).

The COF values of the corrosion attacked conditions were compared with its respective unattacked conditions (Ref 29) under identical dry sliding conditions and are provided in Table 3. The COF values for the corrosion attacked specimens are lower than that of the values obtained in the respective unattacked specimens. In our previous work, performed on the unattacked specimens of the same conditions, the authors had reported the highest value of steady state friction ($\mu \sim 0.87$) for the T300 specimen under identical sliding conditions (Ref 29). This was attributed to higher value of the stress required to cause the detachment of strongly attached M_3C carbides (nano-sized) from the matrix. Exposure to HNO_3 solution caused attack at the carbide-matrix interface regions, leading to dislodgement of the carbides, both undissolved and formed during the tempering from the austenitized and the T300 matrix (Fig. 2a, b, c, d, e, f, g and h). This dislodgement of carbides effectively decreased the contribution of abrasion component of friction in the austenitized and the T300 specimens, resulting in almost same COF values (Ref 36, 37). The severe attack (dislodgement of carbides and loosely held attacked interfaces (Fig. 2e and f) in T550 specimen resulted further decrease in

COF value (0.36), as shown in Table 3. As shown in Figs. 2(g) and (h) and 3(d), T700 specimen had uniform dissolution of the matrix; however, the dislodgement of the carbides is relatively lesser than that in the other tempering conditions. The presence of the undissolved and submicroscopic carbides on the attacked surface of T700 specimen contributed in the abrasion friction and led to increase in the COF value as compared to the other conditions (Ref 12). Apart from this, the presence of surface films developed on the austenitized, T300 and T550 specimens (confirmed by Raman spectroscopy and presented in Sect. 3.4), might have contributed in decreasing the COF as these oxide films reported to be act as solid lubricant (Ref 13).

3.3 Wear behavior

Figure 5(a), (b), (c) and (d) shows the typical 3D profiles and 2D wear depth profiles for the austenitized and the tempered conditions after dry sliding. Average wear depth values (from three experiments) for the corrosion attacked specimens were compared with that of respective unattacked specimens (Ref 29) under identical dry sliding conditions and are provided in Table 4.

Material pile up is not considered in wear depth calculations. As shown in Fig. 5(a) and (b) and Table 4, negligible amount of material removal was observed in attacked specimens of the austenitized and the T300 conditions as compared to their respective unattacked specimens. On the contrary (as shown in Fig. 5c and d and Table 4), increased wear depth for T550 and T700 in attacked specimens compared to that of their unattacked specimens was obtained. Since wear is a surface phenomenon, any surface modifications (due to corrosion attack in the present case) definitely cause significant changes in the wear response of the system (Ref 34, 39). Specific wear rates (k) for the austenitized and the tempered conditions were calculated (from profilometry data), and their average values are presented in Table 4. Descending order k for different studied conditions is:

$$k_{T700} > k_{T550} > k_{T300} \sim k_{Aust.}$$

Significant increase in the k value was observed for T700 (15 times) and T550 (12 times) conditions as compared to the austenitized and the T300 conditions as shown in Table 4. This suggests that the attacked surfaces of the austenitized & the T300 conditions display lower material loss in dry sliding, compared to IGC/inter lath attacked T550 and uniformly corroded T700 surfaces. Specific wear rate (k) is a useful parameter to interpret the severity (mild, severe or transition) of

Table 3 Comparison between the steady state COF (μ) values of unattacked & corrosion attacked conditions of the austenitized and the tempered 13 wt.% Cr MSS under identical dry sliding conditions

Material	Average steady state COF				Remark
	Unattacked (Ref 26)		Corrosion attacked		
13 wt.% Cr MSS condition	μ	Variation for min. and max.	μ	Variation for min. and max.	Extent of reduction in COF for corrosion attacked compared to unattacked condition, %
Austenitized	0.76	20 %	0.44	72 %	42
T300	0.87		0.40		54
T550	0.72		0.36		50
T700	0.74		0.62		16

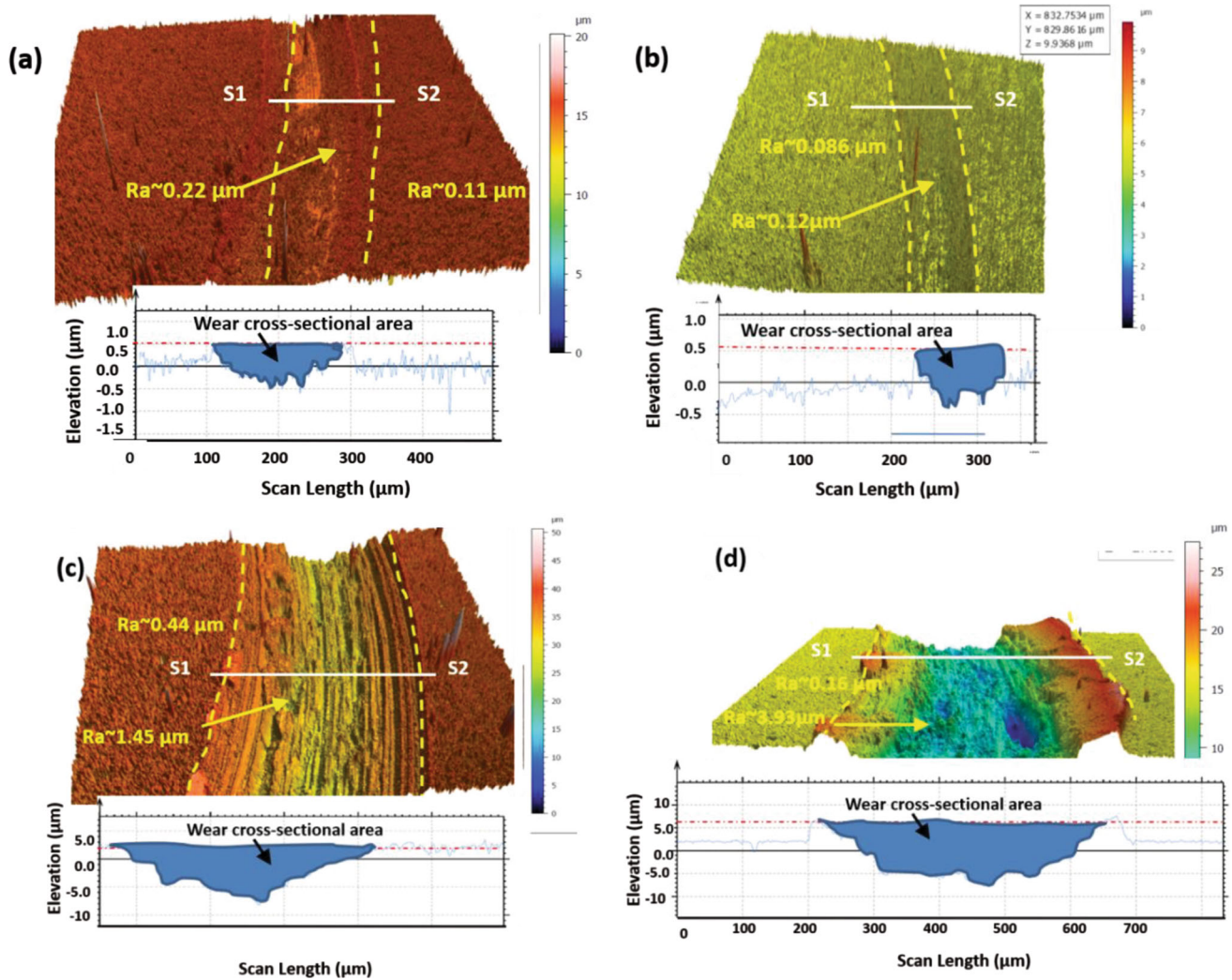


Fig. 5 Profilometric (3D/2D) images of the wear track developed on 13 wt.% Cr MSS in corrosion attacked conditions, (a) Austenitized, (b) T300, (c) T550 and (d) T700 after subjecting to HNO_3 immersion followed by dry sliding. **yellow dotted lines in the images shown to indicate wear track boundaries

Table 4 Comparison of average wear depth and specific wear rates for unattacked and corrosion attacked conditions of austenitized and tempered 13 wt.% Cr MSS under dry sliding against alumina ball

Material		Unattacked (Ref 26)		Corrosion attacked	
13 wt.% condition	Cr MSS	Average wear depth, μm	Specific wear rate $\times 10^{-6}$, k , mm^3/Nm	Average wear depth, μm	Specific wear rate $\times 10^{-6}$, k , mm^3/Nm
Austenitized		1.5	56	0.5	32
T300		2	160	0.5	35
T550		5	208	7	408
T700		4.2	180	7.5	495

abrasive or adhesive wear in dry sliding contacts (Ref 35, 36). Order of the specific wear rate may vary from $10^{-1} \text{ mm}^3/\text{Nm}$ for very severe wear to $10^{-10} \text{ mm}^3/\text{Nm}$ for ultra-mild wear (very favorable conditions) (Ref 35-38). It is generally believed that wear rate is indirectly proportional to the hardness of the softer material in tribo-pair. However, during dry sliding, other factors, e.g., hardness difference with the counterface (Ref 39, 40), fracture resistance (Ref 41), properties/composition of

third bodies (Ref 42, 43) and microstructure (Ref 44, 45) can prompt noticeable changes in the wear rate. Therefore, to interpret the wear response of a particular material pair, in place of jumping to a direct conclusion based on standard relationship between surface hardness and the wear rate (Ref 46), a detailed investigation of wear behavior is required. It has been shown that during dry sliding process, friction and wear often causes mechanical changes, heat transfer and chemical reactions of the

surface material (Ref 47) and these changes usually result in the modifications in the surface properties (formation of tribofilms) and morphologies of materials in contact, being very different from those of the bulk material. In the present work, morphology of the austenitized and the tempered conditions was different at the time of beginning of sliding; therefore, it is expected surfaces to be modified differently and exhibit different wear behavior against same counterface. Quinn (Ref 48) reported reduced friction and wear of metallic materials in dry sliding due to the formation of protective oxide layers by frictional heating within the dry sliding contacts. Though, structure of the oxide layer present depends on temperature & surface conditions at the interface. The breakage of the oxide occurs after reaching a critical thickness and eventually appears as wear debris which in turn affects the wear properties of the sliding interfaces. Properties of debris generated during initial dry sliding of material pair play a very important role in further wear of materials (Ref 12, 15).

3.4 Ex situ Micro-Raman Spectroscopy Analysis on the Wear Tracks

Figure 6(a), (b), (c) and (d) shows the Raman spectra obtained from the wear track region of the pre-corroded austenitized and the different tempered specimens. The fitted

peak positions are compared with the peak positions of different possible compounds that can form on Fe-Cr alloys in (a) an oxidative environment considering the exposure to HNO₃ solution and (b) oxidation during the dry sliding conditions. Wear track regions of the austenitized and the T300 conditions showed the Raman peaks corresponding to Fe₂O₃ and Cr₂O₃, whereas the Raman peaks corresponding to Fe₂O₃ were observed predominantly on the track regions of T550 and T700 specimens as shown in Fig. 6 (Ref 49-51). The austenitized and the T300 specimens also had the low corrosion rates in immersion tests. This is due to the formation of the Cr-rich surface film formation (Ref 8). The higher Cr content in the matrix of the austenitized and the T300 conditions resulted in formation of Cr-rich oxides on the wear track region during dry sliding. The formation of Cr-rich carbides in T550 and T700 specimens decreased the matrix Cr concentration and thereby the formation of Fe-rich oxides on the wear track region of these conditions during dry sliding.

3.5 Wear Mechanisms

Figure 7(a), (b), (c), (e), (f), (g) and (h) shows the typical SEM images showing the morphology of the wear tracks developed on the corrosion attacked austenitized and the tempered specimens under dry sliding conditions. Area marked

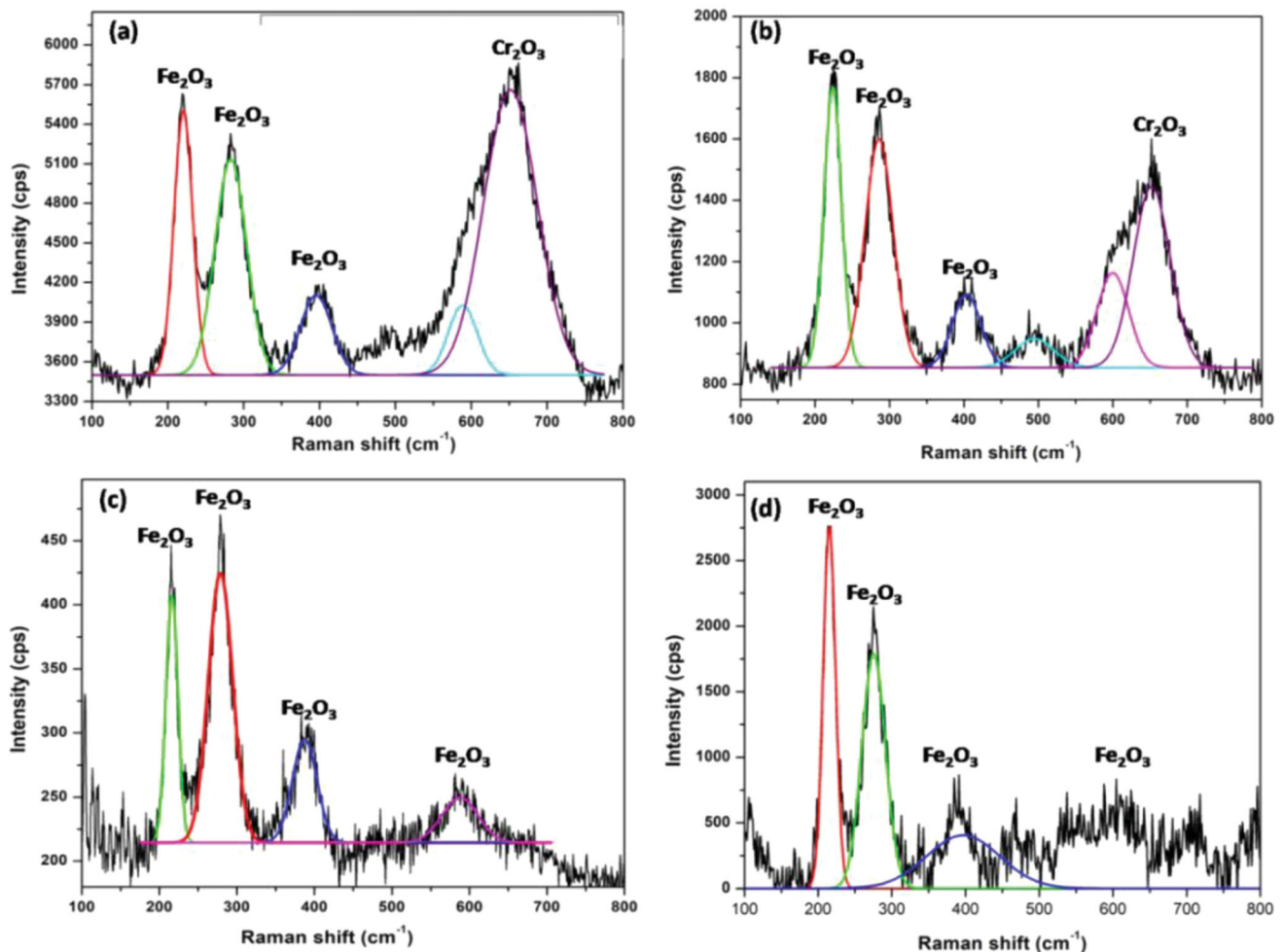


Fig. 6 Raman spectra of worn-out surfaces of 13 wt.% Cr MSS under dry sliding of corrosion attacked conditions, (a) Austenitized, (b) T300, (c) T550 and (d) T700

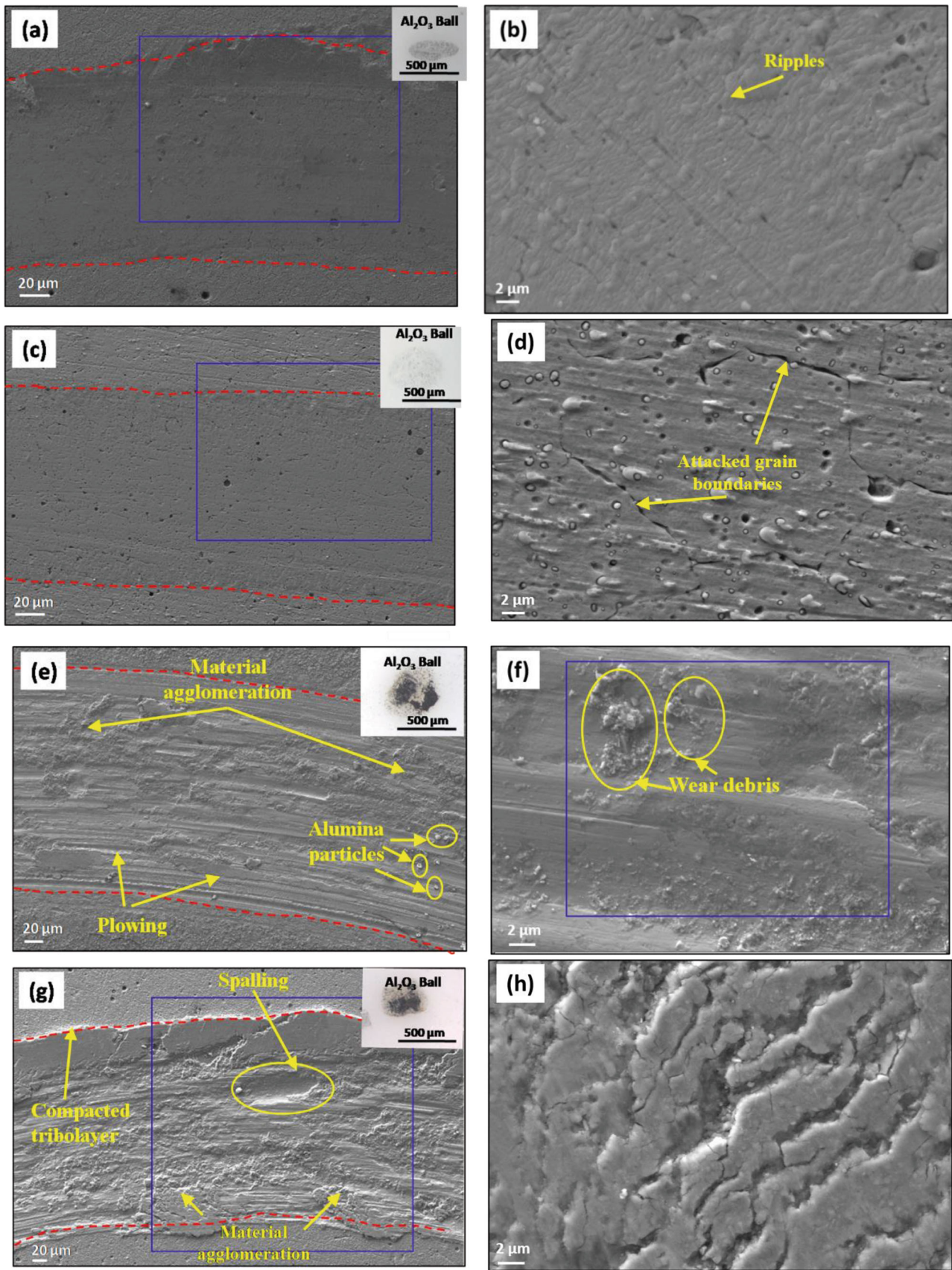


Fig. 7 FE-SEM images of the wear track of 13 wt.% Cr MSS under dry sliding of corrosion attacked conditions, (a)-(b) Austenitized, (c)-(d) T300, (e)-(f) T550 and (g)-(h) T700. The track region used for EDS elemental mapping (for Oxygen) is marked by rectangular area shown in images, and the same is shown in subsequent figures. Red dotted lines in images indicate the wear track boundaries (Color figure online)

in blue color (as shown in Fig. 7) is the region used for acquiring EDS elemental mapping, and only the oxygen (O) elemental map for each condition is shown in Fig. 8(a), (b), (c) and (d) for brevity. The optical image of the worn surface of counterface alumina ball is also shown as an inset in the wear track image of its corresponding condition. The track region of the austenitized specimen is relatively smoother, shiny with the absence of typical wear marks such as plowing, smearing, etc. (Fig. 7a). This is possible in the dry sliding conditions either due to polishing wear or formation of continuous protective tribo-films (Ref 52, 53). Polished worn surfaces are generally appeared as smoother and shiny suggesting low levels of material removal without any plowing, cracks, or visible plastic deformation on the worn surfaces (Ref 52).

Magnified image of the wear track (Fig. 7b) and the EDS elemental (oxygen) mapping (Fig. 8a) confirm that the track region is covered with a continuous oxide layer. Indeed, the surface film was identified as oxides of Cr-rich and Fe using ex situ micro-Raman spectroscopy (Fig. 6a). Tribo-films of Cr-rich oxides with higher hardness and adhesion strength act as a solid lubricant and reduce the friction and wear (Ref 11). Formation of Cr-rich thick and hard tribo-film has increased the load carrying capacity of the austenitized specimen, enabling it to bear applied high contact stress (~ 2.03 GPa). The magnified image (as shown in Fig. 7b) of track region also indicated ripple types of features almost on the middle of the wear track, along with mild plowing marks, which were not observed in

low the magnification image (Fig. 7a) of the wear track. Such features are also observed on the wear track of different materials such as nano-films, ionic crystals and metallic materials after repeated scratching tests in dry sliding (Ref 54, 55). Multiple causes were attributed to the formation of ripples on the track region such as stress-induced micro-fracture, plastic deformation, surface smoothing, shear stresses and/or surface re-hybridization. In the present study, shear stresses (during the repetitive sliding motion between the film and alumina counter body) would have caused surface corrugation or rippling on the tribo-film. The formation of continuous tribo-films (worn surface appeared polished) is the dominating wear mechanism in pre-corroded austenitized condition in dry sliding. The wear mechanism reported for the unattacked austenitized specimen is severe abrasive wear under similar sliding conditions (Ref 29).

Figure 7(c) shows the typical wear track appearance of T300 specimen. The faint plowing marks which are typical features of abrasion wear were observed on the wear track surface in the direction of sliding as shown in Fig. 7(c) and (d). In the dry sliding of unattacked T300 specimen, deep plowing marks in the direction of sliding and wear debris were seen on the wear track (Ref 29). The EDS and Raman analysis of the track region of attacked T300 specimen revealed the presence of the oxide layer similar to that observed on the austenitized specimen. However, the oxide layer formed on T300 specimen did not cover the attacked grain boundaries completely (Fig. 7a) as

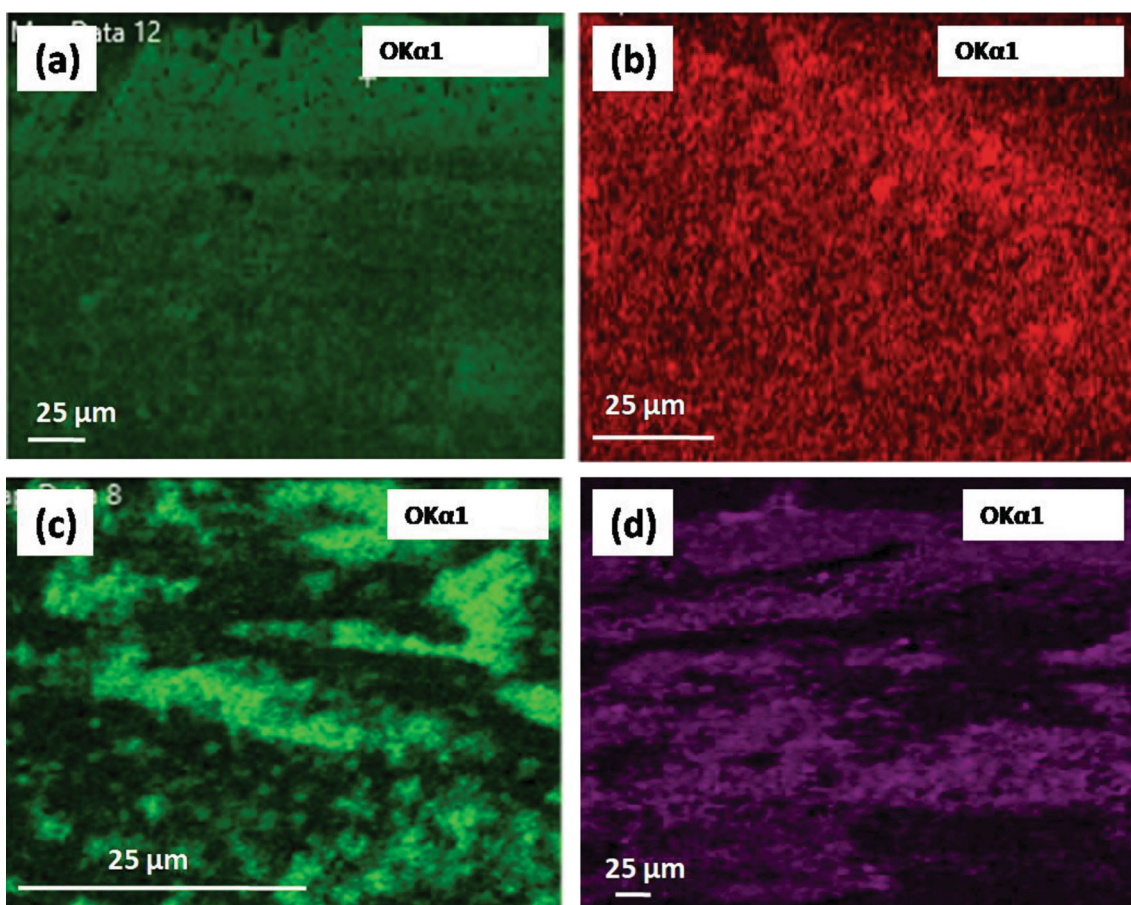


Fig. 8 EDS elemental (O) map of the wear track of 13 wt.% Cr MSS under dry sliding of corrosion attacked conditions, (a) Austenitized, (b) T300, (c) T550 and (d) T700

noticed in austenitized specimen's wear track (Fig. 7b). This is due to the deeper attack along the PAGBs in T300 specimen after exposure to HNO₃ solution (Fig. 3b) or the differences in the thickness of the oxide layer. Indeed, it was due to the lower thickness of the oxide film formed on T300 specimen and is presented in the next section. The faint plowing marks seen in the track region of T300 specimen were due to the friction from the hard particles such as the oxides, fine and undissolved carbides. The transition of wear mechanism from the polishing to mild abrasive wear is evident from the SEM examination of wear track of pre-corroded T300 specimen. In both, pre-corroded austenitized and the T300 conditions, the oxide layer generated during sliding acted as solid lubricant and reduced the friction plus wear rate/damage of the plate/substrate.

The T550 specimen exhibited typical features corresponding to wear mechanisms of adhesion and abrasion as shown in Fig. 7(e) and (f). The material agglomeration, wear debris generated during dry sliding and the alumina particles detached from the counter face alumina ball were shown by arrow marks in the wear track image (Fig. 7e). The material agglomeration occurs when the size of the debris reduces to sufficiently small, so that the small debris adheres and clumps together due to mechanical contacts on the surface (Ref 51-56). As shown in Fig. 2(e) and (f), the surface of the T550 specimen was in IGC/interlath attacked condition with loosely held lath and grains before subjecting it to dry sliding test. Therefore, in the early stage of sliding, the removal of the loosely held material led to generation of wear debris. This debris has begun to agglomerate and adhered on to the surface on repeated sliding. The further sliding test continued on this adhered debris; therefore, the wear features changed to severe adhesion (Fig. 7e). It is to be noted that severe abrasion wear mechanism was observed for dry sliding of unattacked T550 specimen (Ref 29). Wear track for T550 specimen showed the disappearance of IGC and interlath attacked features which were seen just after immersion test (Fig. 2e and f). The wear depth is observed to be $\sim 7 \mu\text{m}$ which is 3.5 times higher than the depth of corrosion attack (Fig. 3c). This shows complete removal of attacked layer during dry sliding. The Raman analysis showed that this debris is predominantly composed Fe-rich oxides, mainly Fe₂O₃. The oxygen EDS map (Fig. 8c) of the region marked in Fig. 7(f) revealed discontinuous Fe-rich oxide layer. Further, few traces of Al at distinct locations were found in the area map analysis (confirmed from analyzing at multiple locations), indicating no significant material transfer from the alumina counterface on to the plate during sliding.

Figure 7(g) and (h) illustrates SEM images of the worn surface of T700 specimen. Material agglomeration, spalling (as shown in Fig. 7g) and presence of compacted layer were observed in the wear track region of pre-corroded T700 specimen. Dry sliding of unattacked T700 specimen had the wear features of plastic deformation and presence of compacted layer (Ref 29). As shown in Fig. 2(g), the surface of T700 specimen had higher amount of the submicroscopic carbides even after exposure to 5 wt.% HNO₃ solution. The carbides played a dominant role on the wear behavior. This was reflected in COF versus time as this condition had higher COF value. The percentage reduction in COF value is about 16% as compared to that on unattacked condition. The wear mechanisms observed for the attacked T700 specimen were also similar to that of unattacked specimen reported in (Ref 29). The magnified SEM image of worn surface as shown in Fig. 7(b) shows the compaction of wear debris with evident boundaries.

The EDS analysis revealed a discontinuous Fe-rich oxide layer as shown in Fig. 8(d). These oxides are mainly Fe₂O₃ as confirmed by Raman spectroscopy. It is believed that embedment of the submicroscopic carbides in these oxide debris affected the wear damage.

3.6 Subsurface (Cross section) Characterization Below the Wear Track of the Austenitized and the Tempered 13 wt.% Cr MSS

The SEM image of the surface below the wear track of austenitized, T300, T550 and T700 specimens is shown in Fig. 9(a), (b), (d) and (e), respectively. Elemental mapping was carried out, and results are presented in Fig. 9(c) and (f) for the austenitized and T550 specimens, respectively. The austenitized specimen (Fig. 9a) exhibited a thick layer ($\sim 4 \mu\text{m}$) of oxide above the wear track. The attack along the PAG boundaries observed after the immersion (refer Fig. 2a) is still visible below the oxide layer (Fig. 9a), confirming that the material removed is less than the depth of attack, during dry sliding. This is because of the lubricating action offered by the oxide film. Before beginning of sliding, the austenitized condition had Cr-rich oxide layer, formed due to exposure to 5 wt.% HNO₃ solution, as confirmed by Raman spectroscopy of the unworn areas. In general, the oxide thickness formed on SSs in aqueous environments at room temperature is about few nano-meters ($\sim 10 \text{ nm}$) (Ref 5, 8). However, almost 4- μm -thick oxide layer was observed in the cross-sectional examination of the wear track for the austenitized condition. This confirms the occurrence of tribochemical reactions and the high flash temperature generated at the asperity contacts on the wear track during sliding led to thickening of the oxide layer (Ref 57).

The surface below the wear track of T300 specimen (Fig. 9b) also showed the presence of a thick oxide layer ($\sim 2.5 \mu\text{m}$), similar to as observed in the austenitized specimen (Fig. 9a). The attack along the PAG boundaries is still evident as shown in Fig. 9(b), confirming the protection offered by the oxide layer generated during the dry sliding. Trevisiol et al. (Ref 58) had observed similar wear behavior in differently tempered martensitic steels because of oxidation during dry sliding (self-lubricating phenomena). The wear behavior under atmospheric conditions would be determined the tribo-films containing Cr₂O₃, Fe₃O₄ and Fe₂O₃.

After dry sliding, subsurface examination of the track region of pre-corroded T550 and T700 specimens showed the absence of thick and continuous oxide layer as shown in Fig. 9(d), (e) and (f). The presence of the carbides in the oxide layer of the worn region is confirmed by EDS elemental mapping (Fig. 9f). Cross-sectional image (Fig. 9e) below the wear track of T700 condition also showed multiple cracks below the wear track after dry sliding for 30 min. The cracks observed up to approximately 20 μm beneath the wear track surface. As shown in Fig. 9(e), material peeling from the surface is also observed below the wear tracks. The material peeling from the surface occurs when the initiated and propagated cracks cause the material to breakthrough (Ref 59). It was also inferred from Fig. 9(e) that a depth of approximately 20 μm was affected by the applied load under dry sliding and caused plastic deformation in this region. The stresses generated under the continuous dry sliding caused the crack initiation and propagation at the defect locations (Ref 39, 48).

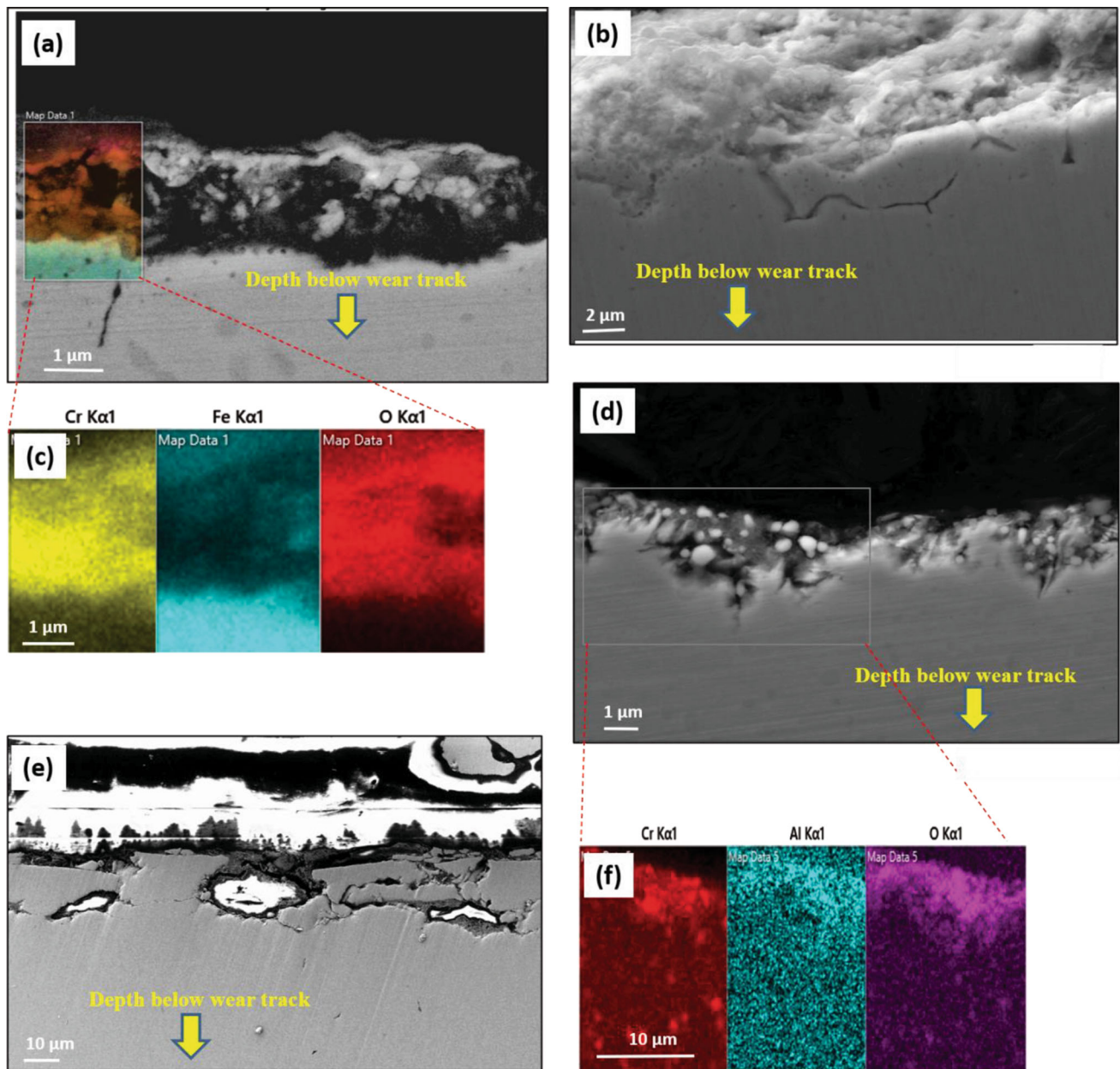


Fig. 9 FE-SEM images of the subsurface of 13 wt.% Cr MSS below the wear track, (a) austenitized, (b) tempered at 300 °C, (c) elemental maps of area selected from (a), (d) tempered at 550 °C, (e) tempered at 700 °C and (f) elemental maps of area selected from (d)

3.7 Protectiveness of Oxide Film on Wear

The pre-corroded specimens of 13 wt.% Cr MSS exhibited a protective oxidational wear mechanism during dry sliding experiments. However, the degree of protectiveness on the wear damage is observed to be dependent on the oxide film coverage. The pre-corroded austenitized and the T300 specimens developed a thick, continuous, adherent Cr-rich oxide layer over the worn surface in dry sliding conditions (Fig. 8a), which protected the surface from direct contact of the counterface. The Cr-rich oxide layer is preventing the wear of material and lowering the friction as compared to the dry sliding of its corresponding unattacked specimen (Ref 29). This is known as self-lubricating effect and is linked to the formation of a tribo-film or oxidation of the contact surface (Ref 13). Further, experimental evidence at different loads, speeds and

durations is necessary to comment on the long-term wear performance of the pre-corroded austenitized and T300 specimens. In opposite to above, the T550 and T700 specimens developed a non-uniformly covered Fe-rich oxide layer on the wear track during dry sliding and thereby adversely affected the wear performance of pre-corroded specimens.

Protectiveness of oxide layer is attributed to its (a) thickness and continuity, (b) relative hardness of oxide to the hardness of counterface materials, (c) the sufficient hardness of substrate to hold the oxide layer and (d) sufficient yield strength and elastic modulus to withstand the applied Hertzian stresses (Ref 14, 22, 23, 33). The hardness of the Fe_2O_3 , Cr_2O_3 and counterface alumina ball are reported to be 6.7 GPa (683 HV), 30 GPa (3060 HV) and 14.3 GPa (1459 HV), respectively (Ref 40, 41, 60-62). Hardness of Cr-rich oxides is much greater than hardness of the counterface alumina ball, therefore able to

provide protection to the austenitized and the T300 specimens. On the contrary, Fe-rich oxides are much softer compared to counterface alumina ball; therefore, the absence of self-lubrication phenomena in T550 and T700 conditions (as opposed to the austenitized and the T300 conditions) is observed. Fe-rich oxide layer got damaged due to its interaction with harder alumina ball and results into formation of loose Fe-rich third bodies. The relative hardness of the loose oxide particles in relation to the material surface in contact (H_O/H_M) has a considerable influence on the wear behavior (Ref 35, 63). The presence of strong Raman peaks of Fe_2O_3 (683 HV) on the worn-out surfaces of T550 (413 HV) and T700 (309 HV) specimens caused the relative hardness (H_O/H_M) of loose oxide particles to matrix as ~ 3.16 and ~ 4.23 , respectively. It has been reported that when the relative hardness of the oxide particles (third bodies) in relation to the matrix in contact is less than 0.9, then mild abrasion prevails (Ref 44), whereas when H_O/H_M value is greater than 1.5, then the wear regime tends to be severe abrasion/adhesion and increases the wear rate significantly. The wear mechanism tends to be between mild and severe wear when H_O/H_M value is between 0.9 and 1.5 (Ref 63). The influence of relative hardness on wear regime transition in different materials has also been reported (Ref 63-65). Thus, observance of higher wear in pre-corroded T550 and T700 specimens compared to unattacked specimens is due to lower hardness of Fe-oxide compared to counterface alumina ball and causes a discontinuous oxide layer and consequently generated loose and hard Fe-rich particles are acting as abrasive agent to softer matrix.

Indeed, our recent tribocorrosion studies on different tempered conditions in nitric acid have shown that the wear-corrosion synergism (tribocorrosion) is an entirely different phenomenon as compared to the wear behavior of corroded/oxidized MSS. These results will be published soon.

4. Conclusions

In this study, the tribology behavior of 13 wt.% Cr MSS in the austenitized and the tempered conditions (at 300, 550, 700 °C) in corrosion attacked (prior immersion of test specimens in 5 wt.% HNO_3 solution at room temperature for 30 min) conditions was studied systematically and compared the behavior with the respective unattacked condition. The unworn/worn-out regions and subsurface were characterized by means of FE-SEM coupled with EDS, 3D/2D profilometry and Raman spectroscopy techniques. The following are the key findings from the present work and brings out the effects of deployment of corrosion attacked surface into tribology applications.

1. Room temperature immersion tests in 5 wt.% HNO_3 solution for 30 min resulted in (a) intergranular corrosion along the prior austenitic boundaries in the austenitized and the tempered at 300 °C specimens, (b) intergranular plus interlath corrosion in 550 °C tempered specimen and (c) heavy uniform corrosion in 700 °C tempered specimen. In ascending order, the corrosion rate is as follows: Tempered at 300 °C \leq Austenitized $<$ Tempered at 700 °C $<$ Tempered at 550 °C and the variation in corrosion rates is attributed to microstructural developments during the austenitization and the tempering.
2. The calculated average steady state coefficient of friction (COF) in descending order is as follows: Tempered at 700 °C ($\mu \sim 0.62$) $>$ Austenitized $>$ Tempered at 550 °C $>$ Tempered at 300 °C ($\mu \sim 0.36$). The austenitized and the tempered at 300 °C conditions exhibited stable COF with time; on the other side, high (along with stick-slip) and moderate fluctuations in COF were observed for tempered at 550 °C and 700 °C conditions.
3. The formation of a continuous Cr-rich oxide layer resulted in a stable COF for the austenitized and the tempered at 300 °C specimens. On the other hand, the presence of discontinuous Fe-rich oxide layer and a large amount of third bodies (wear debris, carbides, iron oxide, alumina, etc.) caused fluctuations in COF for 550 °C and 700 °C tempered specimens.
4. The austenitized and the tempered at 300 °C specimens, despite having an attack along prior austenite grain boundaries surface, displayed the lowest wear depth ($< 1 \mu m$) and mild/transition wear (of the order of $32-35 \times 10^{-6} mm^3/Nm$). This was mainly due to its higher surface hardness and the protective surface film formed during dry sliding. The severe wear ($\sim 10^{-4} mm^3/Nm$) for 550 and 700 °C tempered specimens was due to their lower corrosion resistance and lower hardness, allowing the easy material removal during dry sliding.
5. The predominant wear mechanisms for the austenitized and the tempered 13 wt.% Cr MSS, in attacked condition were established to be:
 - Austenitized and tempered at 300 °C: Polishing plus mild abrasion wear with a Cr-rich uniform tribo-film.
 - Tempered at 550 °C: Severe adhesion plus material agglomeration and transfer, galling, and the presence of loose third bodies.
 - Tempered at 700 °C: Smearing, spalling and compacted tribo-film plus subsurface cracking.

Acknowledgments

The authors are grateful to Dr. Madhumita Goswami and Mr. Anurup Das, Glass and Advanced Materials Division, Bhabha Atomic Research Centre, Mumbai for their help in performing Raman spectroscopy.

References

1. S.J. Zinkle and G.S. Was, Materials Challenges in nuCLEAR energy, *Acta Mater.*, 2013, **61**, p 735–758
2. T. Allen, J. Busby, M. Meyer, and D. Petti, Materials Challenges for Nuclear Systems, *Mater. Today*, 2010, **13**(12), p 14–23
3. M. Narayana Rao, Materials Development for Indian Nuclear Power Programme: An Industry Perspective, *Energy Procedia*, 2011, **7**, p 199–204
4. W.M. Garrison Jr., Stainless steels: martensitic, *encyclopedia of Materials: Science and Technology*, second, K.H.J. Buschow Ed., Elsevier, Oxford, UK, 2001, p 8804–8810
5. S.K. Bonagani, V. Bathula, and V. Kain, Influence of Tempering Treatment on Microstructure and Pitting Corrosion of 13 wt.% Cr Martensitic Stainless Steel, *Corros. Sci.*, 2018, **131**, p 340–354
6. I. Taji, M.H. Moayed, and M. Mirjalili, Correlation Between Sensitization and Pitting Corrosion of AISI 403 Martensitic Stainless Steel, *Corros. Sci.*, 2015, **92**, p 301–308

7. B. Sunil Kumar, V. Kain and B. Vishwanadh, Effect of Tempering Treatments on Microstructure and Intergranular Corrosion of 13 wt.% Cr Martensitic Stainless Steel, *Corrosion*, 2016, **73**(4), p 362–378
8. S.K. Bonagani, V. Kain, V. Bathula, R.H. Banerjee, and S. Tenneti, Electrochemical Behavior and Passive Property of 13Cr Martensitic Stainless Steel in Nitric Acid Solution, *J. Mater. Eng. Perform.*, 2020, **29**(1), p 215–229
9. N. Khare, S.K. Bonagani, P.K. Limaye, and V. Kain, Tribological Study on Tempered 13Cr Martensitic Stainless Steel Susceptible to Interlath/Intergranular Corrosion Under Nitric Acid Sliding Conditions, *Mater. Chem. Phys.*, 2022, **285**, p 126097
10. S. Jacobson and S. Hogmark, Tribofilms- on the crucial importance of tribologically induced surface modifications. In *Book: Recent Developments in Wear Prevention, Friction and Lubrication, Research Signpost* (2010), p. 197–225
11. X. Cheng, Z. Jiang, B. Kosasih, H. Wu, S. Luo, and L. Jiang, Influence of Cr-Rich Oxide Scale on Sliding Wear Mechanism of Ferritic Stainless Steel at High Temperature, *Tribol. Lett.*, 2016, **63**(2), p 1–13
12. M.M. De Oliveira Junior, H.L. Costa, W.M. Silva Junior, and J.D.B. De Mello, Effect of Iron Oxide Debris on the Reciprocating Sliding Wear of Tool Steels, *Wear*, 2019, **426–427**, p 1065–1075
13. Y.G. Cao, C.H. Yin, Y.L. Liang, and S.H. Tang, Lowering the Coefficient of Martensite Steel by Forming a Self-Lubricating Layer in Dry Sliding Wear, *Mater. Res. Express*, 2019, **6**, p 055024
14. Y. Chen, Y. Tang, H. Zhang, and L. Fu, Effect of Chromium on Oxidation in Wear of Surface Nanocrystalline Martensite Steel, *Tribol. Lett.*, 2016, **7**, p 61
15. P.J. Blau, Mechanisms for Transitional Friction and Wear Behavior of Sliding Metals, *Wear*, 1981, **72**, p 55
16. K. Chu, F. Ren, W. Zhu, C. Zhao, P. Bellon, and R.S. Averback, Sliding Wear Induced Subsurface Microstructural Evolution in Nanocrystalline Nb-Ag Binary Alloys and Its Impact on Tribological Performance, *Wear*, 2017, **392–393**, p 69–76
17. S. Jacobson and S. Hogmark, Surface Modifications in Tribological Contact, *Wear*, 2009, **266**, p 370–378
18. S. Masuko, T. Iijima, A. Terawaki, S. Suzuki, T. Aoki, S. Nogi, and S. Obara, Effect of Surface Oxide Layer of Steel on the Tribological Characteristics of Load-bearing Additives for Multiply-Alkylated Cyclopentane Oil Under High Vacuum, *Tribol. Lett.*, 2013, **51**(1), p 115–125
19. K.L. Dahm, E. Torskaya, I. Goryacheva, and P.A. Dearnley, Tribological effects on subsurface interfaces, *Proc. Inst. Mech. Eng. P. I. Mech. Eng. J-J Eng.*, 2007, **221**, p 345
20. L.G. Korshunov and N.L. Chernenko, Effect of Friction-Induced Deformation on the Structure, Microhardness, and Wear Resistance of Austenitic Chromium–Nickel Stainless Steel Subjected to Subsequent Oxidation, *Phys. Met. Metallogr.*, 2016, **117**, p 307–313
21. S.Q. Wang, M.X. Wei, F. Wang, X.H. Cui, and C. Dong, Transition of Mild Wear to Severe Wear in Oxidative Wear of H21 Steel, *Tribol. Lett.*, 2008, **32**(2), p 67–72
22. M.X. Wei, S.Q. Wang, L. Wang, and X.H. Cui, Wear and Friction Characteristics of a Selected Stainless Steel, *Tribol. Trans.*, 2011, **54**(6), p 840–848
23. A. Dalmau, C. Richard, and A.I. Muñoz, Degradation Mechanisms in Martensitic Stainless Steels: Wear, Corrosion and Tribocorrosion Appraisal, *Tribol. Int.*, 2018, **121**, p 167–179
24. A. Gassner, H. Palkowski, C. Müller, J. Wilde, and H. Mozaffari-Jovein, Effect of Microstructural Evolution During Dry Sliding on the Corrosion Behaviour of Martensitic Stainless Steel, *IJMR*, 2022, **113**(9), p 820–832
25. Z. Dai, S. Jiang, B. Wu, L. Ning, S. Li, and D. Duan, Synergism Between Wear and Corrosion of Cr26Mo1 Ferrite Stainless Steels in 0.5 mol/L of Sulfuric Acid, *Tribol. Int. Part*, 2023, **A178**, p 108007
26. R. Bateni, J.A. Szpunar, X. Wang, and D.Y. Li, Wear and Corrosion of Medium Carbon Steel and 304 Stainless Steel, *Wear*, 2006, **260**(1–2), p 116–122
27. A.N. Isfahany, H. Saghafian, and G. Borhani, The Effect of Heat Treatment on Mechanical Properties and Corrosion Behaviour of AISI420 Martensitic Stainless Steel, *J. Alloy Compd.*, 2011, **509**, p 3931–3936
28. K. Chandra, V. Kain, N. Srinivasan, I. Samajdar, and A.K. Balasubrahmanian, Temper Embrittlement and Corrosion Behaviour of Martensitic Stainless Steel 420, *Century Stainl. Steels*, 2013, **794**, p 757–765
29. N. Khare, S.K. Bonagani, P.K. Limaye, and V. Kain, Effect of Tempering on Tribological Properties of 13Cr Martensitic Stainless Steel and Alumina Material Pair in Dry Sliding, *Tribol. Trans.*, 2021, **64**, p 693–707
30. J.Y. Park and Y.S. Park, The Effects of Heat-Treatment Parameters on Corrosion Resistance and Phase Transformations of 14Cr–3Mo Martensitic Stainless Steel, *Mater. Sci. Eng. A*, 2007, **449–451**, p 1131–1134
31. B. Qin, Z.Y. Wang, and Q.S. Sun, Effect of Tempering Temperature on Properties of 00 Cr 16 Ni 5Mo Stainless Steel, *Mater. Charact.*, 2008, **59**, p 1096–1100
32. S.K. Bonagani, V. Kain, N.N. Kumar, and H. Donthula, Effect of Austenitization-Cooling on Microstructure and Localized Corrosion Behavior of 13Cr Martensitic Stainless Steel, *J. Mater. Eng. Perform.*, 2021, **30**, p 2291–2299
33. A. Erdemir, M. Halter, and G.R. Fenske, Preparation of Ultralow-Friction Surface Films on Vanadium Diboride, *Wear*, 1997, **205**(1), p 236–239
34. I.M. Hutchings, *Tribology: Friction and Wear of Engineering Materials*, CRC Press, London, 1992
35. J. Williams, *Engineering Tribology*, Cambridge University Press, Cambridge, UK, 1994
36. W.A. Glaeser, in *ASM Handbook: Friction, Lubrication, and Wear Technology* ed by P.J. Blau (ASM Int., 1992), p. 812–815
37. G.W. Stachowiak and A.W. Batchelor Eds., *Engineering Tribology*, Fourth. Butterworth-Heinemann, Boston, 2014, p 293–370
38. R. Sahli, G. Pallares, C. Ducotet, B. Ali, S. Al Akhrass, M. Guibert, and J. Scheibert, Evolution of Real Contact Area Under Shear and the Value of Static Friction of Soft Materials, *Proc. Natl. Acad. Sci.*, 2018, **115**(3), p 471–476
39. A.C. Bozzi and J.D.B. de Mello, Wear Resistance and Wear Mechanisms of WC Thermal Sprayed Coatings in Three-Body Abrasion, *Wear*, 1999, **233–235**, p 575–587
40. C.C. Viafara and A. Sinatora, Influence of Hardness of the Harder Body on Wear Regime Transition in a Sliding Pair of Steels, *Wear*, 2009, **267**, p 425–432
41. T. Akagaki and D.A. Rigney, Sliding Friction and Wear of Metals in Vacuum, *Wear*, 1991, **149**, p 353–374
42. T.E. Fischer, Z. Zhu, H. Kim, and D.S. Shin, Genesis and Role of Wear Debris in Sliding Wear of Ceramics, *Wear*, 2000, **245**, p 53–60
43. M. Cocks, Wear Debris in the Contact Between Sliding Metals, *J. Appl. Phys.*, 1958, **29**, p 1609–1610
44. M. Ulutan, M. Mustafa Yildirim, S. Buytoz, and O.C. Elik, Microstructure and Wear Behavior of TiG Surface-Alloyed AISI 4140 Steel, *Tribol. Trans.*, 2011, **54**, p 67–79
45. Y. Wang and T. Lei, Wear Behavior of Steel 1080 with Different Microstructures During Dry Sliding, *Wear*, 1997, **36**(2), p 213–217
46. J.F. Archard, Contact and Rubbing of Flat Surfaces, *J. Appl. Phys.*, 1953, **24**, p 981–988
47. R.A. García-León, J. Martínez-Trinidad, R. Zepeda-Bautista, I. Campos-Silva, A. Guevara-Morales, J. Martínez-Londoño, and J. Barbosa-Saldaña, Dry Sliding Wear Test on Borided AISI 316L Stainless Steel Under Ball-on-Flat Configuration: A Statistical Analysis, *Tribol. Inter.*, 2021, **157**, p 106885
48. T.F.J. Quinn, Review of Oxidational Wear: Part I: The Origins of Oxidational Wear, *Tribol. Inter.*, 1983, **16**(5), p 257–271
49. W. Dai, B. Kheireddin, H. Gao, and H. Liang, Roles of Nanoparticles in Oil Lubrication, *Tribol. Int.*, 2016, **102**, p 88–98
50. W. Xia, J. Zhao, H. Wu, S. Jiao, and Z. Jiang, Effects of Oil-in-Water Based Nano Lubricant Containing TiO₂ Nanoparticles on the Tribological Behaviour of Oxidised High-Speedsteel, *Tribol. Int.*, 2017, **110**, p 77–85
51. S. Ningshen, U.K. Mudali, S. Ramya and B. Raj, Corrosion Behaviour of AISI type 304L Stainless Steel in Nitric Acid Media Containing Oxidizing Species, *Corros. Sci.*, 2011, **53**(1), p 64–70
52. K. Kato and G.E. Totten Eds., *Polishing Wear, Friction, Lubrication, and Wear Technology*, Vol 18 ASM International, Almere, 2017
53. R.A. García-León, J. Martínez-Trinidad, I. Campos-Silva, U. Figueroa-López and A. Guevara-Morales, Development of Tribological Maps on Borided AISI 316L Stainless Steel Under Ball-on-Flat Wet Sliding Conditions, *Tribol. Int.*, 2021, **163**, p 1–14
54. A. Socoliuc, E. Gnecco, R. Bennewitz and E. Meyer, Ripple Formation Induced Inlocalized Abrasion, *Phys. Rev. B.*, 2003, **68**, p 1154161–1154164

55. A.E. Filippov, V.L. Popov and M. Urbakh, Mechanism of wear and ripple formation induced by mechanical action of an atomic force microscope tip, *Phys. Rev. Lett.*, 2011, **106**, p 025502-1–025502-4
56. V. Podgursky, T. Hantschel, A. Bogatov, E. Kimmari, M. Antonov, M. Viljus, V. Mikli, M. Tsigkourakos, W. Vandervorst, J.G. Buijnsters, A.T. Raadik, and P. Kulu, Rippling on Wear Scar Surfaces of Nanocrystalline Diamond Films After Reciprocating Sliding Against Ceramic Balls, *Tribol. Lett.*, 2014, **55**(3), p 493–501
57. A. Ravikiran and B.N.P. Bai, Influence of Speed on the Tribochemical Reaction Products and the Associated Transitions for the Dry Sliding of Silicon Nitride Against Steel, *J. Am. Ceram. Soc.*, 1995, **78**(11), p 3025–3032
58. C. Trevisiol, A. Jourani and S. Bouvier, Effect of Microstructures with the Same Chemical Composition and Similar Hardness Levels on Tribological Behavior of Low Alloy Steel, *Tribol. Int.*, 2018, **127**, p 389–403
59. F.H. Stott and G.C. Wood, Influence of Oxides on Friction and Wear of Alloys, *Tribol. Int.*, 1978, **11**(4), p 211–218
60. T. Jøgiaas, A. Tarre, H. Mändar, J. Kozlova and A. Tamm, Nanoindentation of Chromium Oxide Possessing Superior Hardness among Atomic-Layer-Deposited Oxides, *Nanomaterials*, 2022, **12**, p 82
61. M.M. Taheri, Q. Yang, Y. Li, and J.C. Gomez, The Effect of Deposition Parameters on the Structure and Mechanical Properties of Chromium Oxide Coatings Deposited by Reactive Magnetron Sputtering, *Coatings*, 2018, **8**, p 111
62. T. Amano, M. Okazaki, Y. Takezawa, A. Shiino, M. Takeda, T. Onishi, K. Seto, A. Ohkubo, and T. Shishido, Hardness of Oxide Scales on Fe-Si Alloys at Room and High-Temperatures, *Mater. Sci. Forum*, 2006, **522–523**, p 469–476
63. A. Wirth, D. Eggleston, and R. Whitaker, A fundamental tribochemical study of the third body layer formed during automotive friction braking, *Wear*, 1994, **179**(1), p 75–81
64. K.H. Zum Gahr, *Microstructure and Wear of Materials*, Elsevier, New York, USA, 1987
65. K. Kato and K. Adachi, Wear mechanisms, *Modern Tribology*. B. Bhushan Ed., CRC Press, London, 2000

Publisher's Note Springer Nature remains neutral with regard to jurisdictional claims in published maps and institutional affiliations.

Springer Nature or its licensor (e.g. a society or other partner) holds exclusive rights to this article under a publishing agreement with the author(s) or other rightsholder(s); author self-archiving of the accepted manuscript version of this article is solely governed by the terms of such publishing agreement and applicable law.